Passive Q-switching of a Tm3+:LiYF4 waveguide laser by Cr2+:ZnSe and Co2+:ZnSe saturable absorbers

Pavel Loiko, Rémi Soulard, Gurvan Brasse, Lauren Guillemot, A. Braud, Blandine Guichardaz, Ammar Hideur, Patrice Camy

Version of Record: https://www.sciencedirect.com/science/article/pii/S0925346720304596
Manuscript_582a0b71b2750974c68670d736e6b0bb

Passive Q-switching of a Tm^{3+}:$LiYF_4$ waveguide laser by Cr^{2+}:ZnSe and Co^{2+}:ZnSe saturable absorbers

Pavel Loiko[a], Rémi Soulard[a], Gurvan Brasse[a], Lauren Guillemot[a], Alain Braud[a], Blandine Guichardaz[b], Ammar Hideur[c], and Patrice Camy[a,*]

[a]*Centre de recherche sur les Ions, les Matériaux et la Photonique (CIMAP), UMR 6252 CEA-CNRS-ENSICAEN, Université de Caen, 6 Boulevard du Maréchal Juin, 14050 Caen Cedex 4, France*
[b]*Department of Optics, FEMTO-ST Institute, Route de Gray, 25030 Besançon Cedex, France*
[c]*CORIA UMR6614, CNRS-INSA-Université de Rouen, Normandie Université, Avenue de l'université, BP. 12, 76801 Saint Etienne du Rouvray, France*

**Corresponding author, e-mail: patrice.camy@ensicaen.fr*

Abstract. A Tm^{3+}:$LiYF_4$ / $LiYF_4$ channel waveguide laser produced by Liquid Phase Epitaxy and diamond-saw dicing is passively Q-switched by Cr^{2+}:ZnSe and Co^{2+}:ZnSe saturable absorbers. For Cr^{2+}:ZnSe, the laser generated a maximum average output power of 0.59 W at 1876.5 nm with a slope efficiency of 36.1% (with respect to the absorbed pump power) and a linearly polarized output (π-polarization). The pulse characteristics (duration / energy) were 9 ns / 2.1 μJ at a repetition rate of 0.29 MHz. The laser performance was modelled within a "slow" saturable absorber model showing good agreement with the experiment. We also revisited Co^{2+}:ZnSe for passive Q-switching applications in the spectral range of ~2 μm. It allowed to operate the laser in a high-repetition-rate regime (0.91 MHz) while preserving the benefits of short pulses (30 ns / 0.9 μJ). For Co^{2+}:ZnSe, the average output power of the waveguide laser reached 0.81 W with a record-high slope efficiency of 49.6%.

Keywords: waveguide laser; thulium ions; saturable absorber; zinc selenide; passive Q-switching.

1. Introduction

Waveguide (WG) lasers operating in the eye-safe spectral range of ~2 μm are of interest for spectroscopy, bio- and environmental sensing, telecom applications and soft material processing. Such coherent sources are achieved using trivalent thulium (Tm^{3+}) or holmium (Ho^{3+}) ions. Due to the typically large Stark splitting of the ground-state ($^3H_6$), Tm^{3+} ions feature broadband emission slightly below 2 μm (the $^3F_4 \rightarrow {}^3H_6$ transition) [1] overlapping with the absorption lines of H_2O molecules. Moreover, they can be excited at ~0.8 μm (to the $^3H_4$ state) using high-power AlGaAs laser diodes or high-brightness Ti:Sapphire lasers [1,2]. Due to the efficient cross-relaxation (CR) process for adjacent Tm^{3+} ions even at moderate doping levels, $^3H_4(Tm_1) + {}^3H_6(Tm_2) \rightarrow {}^3F_4(Tm_1) + {}^3F_4(Tm_2)$, the pump quantum efficiency can reach 2 greatly improving the laser efficiency and reducing detrimental heat loading [3].

Efficient and power scalable Tm WG lasers are known [3-6]. Liquid Phase Epitaxy (LPE) is one of the most reliable methods to produce Tm^{3+}-doped waveguiding crystalline thin films for laser applications [5]. So far, LPE has been applied for various Tm^{3+}-doped materials, such as cubic $Tm^{3+}:Y_3Al_5O_{12}$ [5], tetragonal $Tm^{3+}:LiYF_4$ [7] or monoclinic $Tm^{3+}:KY(WO_4)_2$ [8]. The as-grown films may be used in planar WGs lasers while their microstructuring leads to fabrication of channel WG lasers. The latter are more desirable because of single-transverse mode behavior, lower laser threshold, stronger confinement of the laser mode and thus higher intracavity light intensity. So far, different methods such as reactive ion etching [9] or diamond-saw dicing [7,10] were used for producing channel WGs in LPE-grown films. Recently, a continuous-wave $Tm^{3+}:LiYF_4$ / $LiYF_4$ channel WG laser delivering 1.30 W at 1880 nm with a slope efficiency of 79.7% and a laser threshold of 70 mW was reported [7].

Passive Q-switching is a well-known method to generate ns-long pulses in solid-state lasers. This regime is ensured by insertion into the cavity of a saturable absorber (SA). A SA is a nonlinear optical element which exhibits increased transmission under high incident light fluence / intensity (called bleaching or absorption saturation). According to the ratio between the recovery time of the initial absorption τ_{rec} and the characteristic time of pulse formation $\Delta\tau$, the SAs can be classified as "fast" ($\tau_{rec} << \Delta\tau$) and "slow" ($\tau_{rec} > \Delta\tau$). Particularly "slow" SAs are useful for generation of short [11] and high-energy [12] pulses at relatively low repetition rates. State-of-the-art "slow" SAs are based on transition-metal ion-doped crystals [13].

Nowadays, chalcogenide crystals (ZnS and ZnSe) doped with chromium (Cr^{2+}) ions [14] are widely used as "slow" SAs of bulk solid-state lasers emitting in the spectral range of ~2 μm [12,15]. They feature broadband and intense absorption bands due to the $^5T_2 \rightarrow {}^5E(^5D)$ transition of Cr^{2+} ions in tetrahedral (T_d) sites, low saturation fluence, almost zero excited-state absorption (ESA) [16] and acceptable laser-induced damage thresholds (LIDTs) [17]. The host materials, in their turn, provide good transparency in the near-IR and attractive thermal properties. Cr^{2+}-doped zinc selenide (ZnSe), as compared to its ZnS counterpart, provides a red-shift of the absorption band [15].

Despite broad applications of Cr^{2+}-doped chalcogenides as SAs of ~2 μm bulk lasers, they have been barely studied in WG oscillators. The only report presented a $Tm^{3+}:KY(WO_4)_2$

planar WG laser passively Q-switched by a Cr^{2+}:ZnS SA and generating rather long pulses (1.2 μs / 120 nJ) [8]. The output power was as low as 1.2 mW at ~1.84 μm.

In the present work, we aimed to demonstrate efficient and power-scalable passively Q-switched (PQS) Tm channel WG lasers employing transition-metal ion-doped ZnSe crystals as SAs. In addition to Cr^{2+}:ZnSe, we used its cobalt (Co^{2+})-doped counterpart [18,19] which was not studied previously for the ~2 μm spectral range.

2. Experimental

2.1. Waveguide fabrication

As a laser gain material, we selected Tm^{3+}-doped lithium yttrium fluoride ($LiYF_4$) single-crystalline thin films. Tetragonal Tm^{3+}:$LiYF_4$ is known for laser emission at ~1.9 μm [6,20]. It features good thermal properties, linearly polarized laser output [21], strong CR and good energy storage capabilities (upper laser level lifetime of ~10 ms) [22] which is attractive for attaining high pulse energies under PQS operation [22].

The Tm^{3+},Gd^{3+}:$LiYF_4$ single-crystalline thin films were grown on (001)-oriented undoped bulk $LiYF_4$ substrates by LPE using LiF as a solvent [7]. Codoping with optically passive Gd^{3+} ions was implemented to increase the refractive index difference between the active layer and the substrate Δn, estimated to be $2.3\pm0.5\times10^{-3}$ at 1.88 μm for π-polarization [7]. The actual Tm^{3+} doping level was 6.2 at.% (ion density: $N_{Tm} = 8.6\times10^{20}$ cm^{-3}). The top surface of the film was polished to laser quality to reach a thickness of 30 μm.

The epitaxies were microstructured by diamond-saw dicing [7,10] resulting in fabrication of surface channel (ridge) WGs, with a square cross-section of 30×30 μm^2 and a length of 8.0 mm (for light propagation along the crystallographic ***a***-axis, ***a***-cut), Fig. 1. The WG propagation losses, estimated from CW laser performance by applying the Caird analysis [24], amounted to 0.27 ± 0.1 dB/cm.

2.2. Laser set-up

The Tm^{3+}:$LiYF_4$ / $LiYF_4$ epitaxy was mounted on a passively cooled Cu-holder using a silver paste to improve the thermal contact. The laser cavity was composed by a flat pump mirror (PM) coated for high transmission (HT, T = 96%) at ~0.78 μm and high reflection (HR) at 1.87–2.3 μm, and a flat output coupler (OC) with a transmission T_{OC} = 50% at the laser wavelength, Fig. 2. A transmission-type SA was inserted between the sample and the OC at a normal incidence. The cavity mirrors, the WG and the SA were all placed next to each other with minimum air gaps. No index-matching liquid was used to avoid optical damage.

The WG was pumped by focused output of a CW Ti:Sapphire laser (model 3900S, Spectra Physics) delivering up to 3.2 W at 783 nm with a spatially single-mode output (M^2 ≈1). For this, a spherical lens (focal length f = 50 mm, transmission at the pump wavelength T = 88%) was used. The pump polarization in the WG corresponded to π. The measured pump coupling efficiency was 87±1%. The pumping was in a single-pass. The pump absorption measured at the threshold pump power for PQS operation was 70±1%. The pump power incident on the WG was varied by a rotatory half-wave plate and a Glan-Taylor polarizer.

The laser output was filtered from the residual pump by a cut-off filter. The laser spectra were measured using an optical spectrum analyzer (OSA, model AQ6375B, Yokogawa, spectral resolution: 0.1 nm) and the temporal behavior was studied using a fast InGaAs photodetector (model UPD-5N-IR2-P, rise time: <200 ps) and an 8 GHz digital oscilloscope (DSA70804B, Tektronix).

2.3. Saturable absorbers

Two SAs made of Cr^{2+}:ZnSe and Co^{2+}:ZnSe crystals were used. In ZnSe, the transition-metal ions are replacing the Zn^{2+} cations in tetrahedral (T_d) sites [14]. This leads to high ground-state absorption (GSA) transition cross-sections, σ_{GSA}, Fig. 3. The broad absorption band of Cr^{2+} ions centered at ~1.76 μm is due to the $^5T_2 \rightarrow {}^5E(^5D)$ transition. At 1.88 μm, $\sigma_{GSA} = 0.69\times10^{-18}$ cm^2. Weaker absorption band of Co^{2+} ions is centered at 1.60 μm and it is related to the $^4A_2 \rightarrow {}^4T_1(^4F)$ transition. The corresponding $\sigma_{GSA} = 0.22\times10^{-18}$ cm^2 at 1.88 μm.

The SAs had a thickness (t) of 1.01 mm and 1.91 mm for Cr^{2+}:ZnSe and Co^{2+}:ZnSe, respectively. Both their sides were polished to laser quality and antireflection (AR) coated for 1.5-1.9 μm. The small-signal (unsaturated) absorption at the laser wavelength T_{SA} was 97.0% and 99.2%, respectively. The key properties of the SAs are summarized in Table 1.

3. Results and Discussion

3.1 Laser performance

At first, we characterized the laser performance in the CW regime (when removing the SA from the cavity). The Tm^{3+}:$LiYF_4$ WG laser generated a maximum output power of 1.30 W at 1877-1883 nm with a slope efficiency η = 79.7% (*vs*. the absorbed pump power P_{abs}) and a laser threshold of 65 mW.

When inserting the SAs, a stable passive Q-switching was achieved for the whole range of pump powers. For the Cr^{2+}:ZnSe SA, the average output power reached 0.59 W at 1876.5 nm with η = 36.1%, Fig. 4(a). The Q-switching conversion efficiency with respect to the CW regime η_{conv} was 45.4% and the laser threshold was at P_{abs} = 155 mW. Higher average output power was achieved for the Co^{2+}:ZnSe SA, namely 0.81 W at 1877.7 nm corresponding to η = 49.6%. The laser threshold was at P_{abs} = 150 mW and the Q-switching conversion efficiency increased to 62.3%. The drop in the laser performance when inserting the SA in the cavity is due to scattering losses in ZnSe and possible non-saturable absorption of transition-metal ions. However, the Co^{2+}:ZnSe SA provided lower stability of the PQS operation. For both CW and PQS lasers, the emission was linearly polarized (π) and the polarization was naturally selected by the gain anisotropy. The input-output dependences were clearly linear showing no detrimental thermal effects. No thermal fracture of the epitaxy nor optical damage of the SAs / cavity mirrors were detected.

The typical laser emission spectra for the CW and PQS lasers are shown in Fig. 4(b). They are centered at ~1.88 μm, in agreement with the gain spectra of Tm^{3+} ions in $LiYF_4$ for π-polarization [22]. For the CW regime, the spectrum was broad and for the PQS operation, it was notably narrowed due to the mode competition [25]. A slight blue-shift of the emission spectra for the PQS laser with respect to the CW one was detected. It is explained by the

quasi-three-level nature of the Tm^{3+} laser scheme: for higher intracavity losses, larger inversion is needed to reach the condition "gain is equal to losses" leading to weaker reabsorption and a blue-shift in the gain spectra.

The pulse characteristics of the PQS lasers are shown in Fig. 5. The pulse duration $\Delta\tau_p$ (determined as full width at half maximum, FWHM) and the pulse repetition frequency (PRF) were measured directly, and the pulse energy was calculated: $E_{out} = P_{out}/PRF$ (here, P_{out} is the average output power). Both Cr^{2+}:ZnSe and Co^{2+}:ZnSe (recovery time of initial absorption: τ_{rec} = 5.4 μs and ~100 μs, respectively [16,18]) are "slow" SAs for the designed PQS laser, so that a weak dependence of $\Delta\tau_p$ and E_{out} on the pump power is expected. This is clearly observed for Cr^{2+}:ZnSe: the pulse duration / energy were almost constant above the laser threshold, ~9 ns / 2.1 μJ, and the PRF increased almost linearly from 21 to 290 kHz. The maximum peak power of the PQS laser, $P_{peak} = E_{out}/\Delta\tau_p$, thus reached 0.23 kW.

For Co^{2+}:ZnSe, more notable variation of the pulse characteristics was observed. With the increase of the pump power, the pulse duration shortened from 145 to 30 ns and the pulse energy increased from 0.2 to 0.9 μJ. The PRF was also changing almost linearly, from 0.18 to 0.91 MHz. The peak power reached 0.03 kW. Lower energies and longer pulses achieved with the Co^{2+}:ZnSe SA are due to its lower modulation depth. Probably because of the same reason, the stabilization of the pulse characteristics is achieved at much higher pump power as compared to Cr^{2+}:ZnSe.

The typical oscilloscope traces of the laser emission from the PQS Tm^{3+}:$LiYF_4$ WG laser at the maximum applied pump power are shown in Fig. 6. The single Q-switched pulses have a nearly Gaussian temporal shape. The intensity instabilities and the r.m.s. pulse-to-pulse timing jitter are <15% and <30% for Cr^{2+}:ZnSe and Co^{2+}:ZnSe SAs, respectively. It is known that the stability of PQS operation in compact lasers is affected by heating of the SA by the residual (non-absorbed) pump. In our case, this detrimental effect is greatly suppressed by enough pump absorption in the WG. Lower stability of PQS operation with the Co^{2+}:ZnSe SA is due to its absorption at 0.67-0.8 μm originating from the $^4A_2(^4F) \rightarrow {}^4T_1(^4P)$ transition of Co^{2+} ions in T_d sites [18,19] and overlapping with the pump wavelength.

The output mode of the Tm^{3+}:$LiYF_4$ WG laser was measured. The equivalent size of the mode at the OC amounted to $2w_L$ = 30±3 μm (at the $1/e^2$ intensity level, w_L – the mode radius) and the 1D intensity profiles were well fitted with a Gaussian distribution. The measured $M^2_{x,y}$ parameters were 1.1±0.1 indicating a single-transverse-mode operation.

3.2. Modeling

The criterion for efficient "slow" SA passive Q-switching is the following [27]:

$$X = \frac{\sigma_{GSA}}{\sigma^g_{abs} + \sigma^g_{SE}} \frac{A_g}{A_{SA}} >> 1 \qquad (1)$$

Here, σ_{GSA} is the GSA cross-section of SA, σ^g_{abs} and σ^g_{SE} are the absorption and stimulated-emission (SE) cross-sections of the gain material, respectively, A_g and A_{SA} are the laser mode areas in the gain material and SA, respectively. For the designed WG laser, $A_g \approx A_{SA}$, so that the parameter X is defined mostly by the spectroscopic properties. For Tm^{3+}:$LiYF_4$, σ_{SE} = 0.42×10^{-20} cm^2 and σ_{abs} = 0.07×10^{-20} cm^2 at the wavelength of ~1.88 μm for π-polarization

[22]. Thus, X > 100 for Cr^{2+}:ZnSe and X = 45 for Co^{2+}:ZnSe. A weak dependence of the pulse characteristics on the pump power is observed for $X >> 1$. The determined X values explain the observation of such a dependence when using Co^{2+}:ZnSe, Fig. 5, by relative closeness of the saturation intensities of the gain material and the SA.

The intracavity peak on-axis fluence on the SA can be calculated as [28]:

$$F_{in} = \frac{2 - T_{OC}}{T_{OC}} \frac{2E_{out}}{\pi w_L^2}. \quad (2)$$

Here, the term "2" indicates a Gaussian spatial profile of the laser mode. For the Cr^{2+}:ZnSe and Co^{2+}:ZnSe SA, the maximum F_{in} = 1.78 J/cm^2 and 0.76 J/cm^2, respectively. By comparing these values to the saturation fluence F_S of both SAs, cf. Table 1, we conclude that both SAs are deeply bleached. The determined F_{in} values also represent the lower limit for the LIDT for the studied SAs for ns-long pulses.

The pulse characteristics of the Tm^{3+}:$LiYF_4$ WG laser PQS by the Cr^{2+}:ZnSe SA were calculated within the model of a quasi-three-level gain medium and a "slow" SA [29]. The parameters of the gain material and the SA used for the modeling are listed in the text. The results are shown in Fig. 7. They are in good agreement with the experimental data. For high output coupling, the pulse characteristics are weakly dependent on T_{OC}. However, the use of high T_{OC} (50% in the present work) allowed us to decrease the intracavity fluence on the SA, Eq. (2), and avoid its optical damage. With the increase of the modulation depth of the SA (1 – T_{SA}), the generation of even shorter and more energetic pulses is expected. However, this may be accompanied by a higher probability of optical damage and higher insertion loss of the SA leading to a decrease in the laser slope efficiency.

A similar modeling was also performed for the Co^{2+}:ZnSe SA. A reasonable agreement between the experimental and calculated pulse duration / energy was observed only for the pump powers well above the laser threshold (for P_{abs} >> 1 W), where nearly constant pulse characteristics were observed. Note that this model does not account for the dependence of the pulse characteristics on P_{abs}.

3.3 Discussion

In Table 2, we summarize the results on PQS Tm channel waveguide lasers reported to date. Previously, only "fast" SAs ($\tau_{rec} << \Delta\tau$) were implemented in such lasers. "Fast" SAs allow to obtain higher repetition rates (typically, in the MHz-range) whilst at much lower pulse energies and longer pulse durations [30]. Moreover, the pulse characteristics are strongly dependent on the pump power because of the dynamic bleaching of the SA. Those "fast" SAs were based on carbon nanostructures (graphene [31-33] and single-walled carbon nanotubes – SWCNTs [34]), transition metal dichalcogenides – TMDs (e.g., MoS_2) [33] or topological insulators – TIs (e.g., Bi_2Te_3) [35].

The best results were achieved with a Tm^{3+}:$KLu(WO_4)_2$ WG produced by femtosecond direct laser writing (DLW) and based on an evanescent interaction with surface-deposited SWCNTs [34]. It generated 150 mW at 1847 nm with η = 34.6% and the pulse characteristics were 0.11 μJ / 98 ns at a high repetition rate of 1.42 MHz.

The results achieved in the present work represent the best laser characteristics among all studied PQS Tm channel WG lasers, in terms of the highest output power, slope efficiency, pulse energy and the shortest pulse duration. The main reason for this is the proper selection of the gain material and the SA. Indeed, the gain material (Tm^{3+}:$LiYF_4$) features good thermal properties allowing for power scaling to almost watt-level output power, limited mostly by the available pump source. The long upper laser level ($^3F_4$) lifetime of Tm^{3+} ions (about 10 ms) is a prerequisite for attaining high pulse energies. The selected SAs (Cr^{2+}:ZnSe and Co^{2+}:ZnSe) featuring low saturation fluence, low non-saturable losses and acceptable LIDT, were deeply bleached in the designed laser cavity well satisfying the criterion for "slow" SA PQS, Eq. (1).

Finally, let us comment on formation of the laser mode within the SA. The introduction of the SA into the laser cavity implies that there is a "free space" section of the resonator where the mode guiding is no longer provided by the refractive index contrast (like within the WG itself) and, thus, the mode can expand. Such a situation will inevitably lead to a certain coupling loss between the guided and free space modes after the light leaves the channel and returns back after passing through the SA and being reflected by the output coupler. Such coupling loss in included into the total insertion loss of the SA, expressed by the Q-switching conversion efficiency. Other contributions arise from the scattering losses and non-saturable absorption of the SA, as explained above. To our opinion, the latter factor dominates in the developed oscillator, as an increase of the SA thickness for Co^{2+}:ZnSe (as compared to Cr^{2+}:ZnSe) is not accompanied by a respective drop of the Q-switching conversion efficiency.

The "free space" section of the resonator resembles a microchip laser, where the most common mechanism of the mode formation is the positive (focusing) thermal lens [36]. SAs can exhibit thermal lensing [37,38] due to the residual (non-saturated) absorption both at the pump and laser wavelengths. The thermo-optical properties of a laser material in a free space are expressed by the so-called thermal coefficient of the optical path (TCOP) [39], $W = dn/dT + (n - 1)\alpha$, where dn/dT is the thermo-optic coefficient and α is the coefficient of thermal expansion. For ZnSe, the first term is large and positive ($dn/dT = 5.45\times10^{-5}$ K^{-1} at ~1.88 μm [40]) and dominates over the contribution of thermal expansion ($\alpha = 7.8\times10^{-6}$ K^{-1} [41]). Thus, strong positive thermal lens is expected in ZnSe-based SAs which will stabilize the laser mode in the "free space" section of the resonator and reduce the back-coupling loss. Indeed, microchip Cr^{2+}:ZnSe lasers are known [42].

4. Conclusion

To conclude, we have demonstrated stable and efficient passively Q-switched operation of thulium channel WG lasers using Cr^{2+}- and Co^{2+}-doped ZnSe saturable absorbers capable of producing nanosecond pulses at high average output powers (approaching the watt-level) due to good thermal and spectroscopic properties of Tm^{3+}:$LiYF_4$ used as a gain material, low propagation losses in the fabricated WGs and attractive nonlinear properties of transition-metal ion-doped ZnSe crystals acting as classical "slow" SAs. In particular, for the Cr^{2+}:ZnSe SA, the pulse energy / duration were 2.1 μJ / 9 ns at a repetition rate of 0.29 MHz (average output power: 0.59 W at 1877 nm), representing the record values for any PQS thulium WG lasers reported to date.

We also revisited the Co^{2+}:ZnSe crystal for PQS applications in the spectral range of ~2 μm. Because of the smaller modulation depth and higher saturation intensity (as compared to Cr^{2+}:ZnSe), we operated this SA in a high-repetition-rate regime (PRF = 0.91 MHz) while preserving the benefits of short pulses (0.9 μJ / 30 ns). The average output power of the PQS WG laser in this case was even higher, 0.81 W with a record-high slope efficiency of 49.6%. Co^{2+}:ZnSe may be thus considered as an alternative to "fast" SAs such as graphene as it may provide better laser performance with comparable pulse characteristics.

The studied channel WGs are also of interest for high repetition-rate (GHz-range) mode-locked oscillators.

Acknowledgements

This work was supported by French Agence Nationale de la Recherche (ANR) through the LabEx EMC3 (ANR-10-LABX-09-01), SPLENDID2 (ANR-19-CE08-0028), and the European project "NOVAMAT" co-funded by the Normandy County Council and the European Union within the framework of the Operational Program ERDF/ESF 2014-2020.

References

1. R. C. Stoneman, L. Esterowitz, Efficient, broadly tunable, laser-pumped Tm:YAG and Tm:YSGG cw lasers, Opt. Lett. 15 (1990) 486–488.

2. S. So, J. I. Mackenzie, D. P. Shepherd, W. A. Clarkson, J. G. Betterton, E. K. Gorton, A power-scaling strategy for longitudinally diode-pumped Tm:YLF lasers, Appl. Phys. B 84 (2006) 389–393.

3. K. van Dalfsen, S. Aravazhi, C. Grivas, S. M. García-Blanco, M. Pollnau, Thulium channel waveguide laser with 1.6 W of output power and ~80% slope efficiency, Opt. Lett. 39 (2014) 4380–4383.

4. W. Bolanos, F. Starecki, A. Benayad, G. Brasse, V. Ménard, J.-L. Doualan, A. Braud, R. Moncorgé, P. Camy, Tm:$LiYF_4$ planar waveguide laser at 1.9 μm," Opt. Lett. 37 (2012) 4032–4034.

5. A. Rameix, C. Borel, B. Chambaz, B. Ferrand, D. P. Shepherd, T. J. Warburton, D. C. Hanna, A. C. Tropper, An efficient, diode-pumped, 2 μm Tm:YAG waveguide laser, Opt. Commun. 142 (1997) 239–243.

6. J. I. Mackenzie, S. C. Mitchell, R. J. Beach, H. E. Meissner, and D. P. Shepherd, 15 W diode-side-pumped Tm:YAG waveguide laser at 2 μm, Electron. Lett. 37 (2001) 898–899.

7. P. Loiko, R. Soulard, G. Brasse, J.-L. Doulan, B. Guichardaz, A. Braud, A. Tyazhev, A. Hideur, P. Camy, Watt-level Tm:$LiYF_4$ channel waveguide laser produced by diamond saw dicing, Opt. Express 26 (2018) 24653-24662.

8. W. Bolaños, J. J. Carvajal, X. Mateos, E. Cantelar, G. Lifante, U. Griebner, V. Petrov, V. L. Panyutin, G. S. Murugan, J. S. Wilkinson, M. Aguiló, and F. Díaz, Continuous-wave and Q-switched Tm-doped $KY(WO_4)_2$ planar waveguide laser at 1.84 μm, Opt. Express 19 (2011) 1449–1454.

9. K. van Dalfsen, S. Aravazhi, D. Geskus, K. Wörhoff, and M. Pollnau, "Efficient $KY_{1-x-y}Gd_xLu_y(WO_4)_2:Tm^{3+}$ channel waveguide lasers, Opt. Express 19 (2011) 5277–5282.

10. E. Kifle, P. Loiko, U. Griebner, V. Petrov, P. Camy, A. Braud, M. Aguiló, F. Díaz, X. Mateos, Diamond saw dicing of Thulium channel waveguide lasers in monoclinic crystalline films, Opt. Lett. 44 (2019) 1596-1599.
11. P. Loiko, J.M. Serres, X. Mateos, K. Yumashev, A. Yasukevich, V. Petrov, U. Griebner, M. Aguiló, F. Díaz, Subnanosecond Tm:KLuW microchip laser Q-switched by a Cr:ZnS saturable absorber, Opt. Lett. 40 (2015) 5220-5223.
12. H. Yu, V. Petrov, U. Griebner, D. Parisi, S. Veronesi, M. Tonelli, Compact passively Q-switched diode-pumped Tm:$LiLuF_4$ laser with 1.26 mJ output energy, Opt. Lett. 37 (2012) 2544-2546.
13. A. M. Malyarevich, K. V. Yumashev, Saturable absorbers based on tetrahedrally coordinated transition-metal ions in crystals, J. Appl. Spectr. 76 (2009) 1-43.
14. L. D. DeLoach, R. H. Page, G. D. Wilke, S. A. Payne, W. F. Krupke, Transition metal-doped zinc chalcogenides: spectroscopy and laser demonstration of a new class of gain media, IEEE J. Quantum Electron. 32 (1996) 885-895.
15. T.-Y. Tsai, M. Birnbaum, Q-switched 2-μm lasers by use of a Cr^{2+}:ZnSe saturable absorber, Appl. Opt. 40 (2001) 6633-6637.
16. S. B. Mirov, V. V. Fedorov, D. V. Martyshkin, I. S. Moskalev, M. S. Mirov, V. P. Gapontsev, Progress in mid-IR Cr^{2+} and Fe^{2+} doped II-VI materials and lasers, Opt. Mater. Express 1 (2011) 898-910.
17. P. Loiko, V. Vitkin, S. Balabanov, O. Dymshits, K. Grigorenko, A. Polishchuk, A. Volokitina, X. Mateos, J. M. Serres, E. Gavrishchuk, Saturable absorption properties at 1.54 μm of Cr^{2+}:ZnS prepared by thermal diffusion at hot isostatic pressing, Laser Phys. Lett. 16 (2019) 065801-1-6.
18. T. Y. Tsai, M. Birnbaum, Co^{2+}:ZnS and Co^{2+}:ZnSe saturable absorber Q switches, J. Appl. Phys. 87 (2000) 25-29.
19. A. V. Podlipensky, V. G. Shcherbitsky, N. V. Kuleshov, V. P. Mikhailov, V. I. Levchenko, V. N. Yakimovich, Cr^{2+}:ZnSe and Co^{2+}:ZnSe saturable-absorber Q switches for 1.54-μm Er:glass lasers, Opt. Lett. 24 (1999) 960-962.
20. M. Schellhorn, High-power diode-pumped Tm:YLF laser, Appl. Phys. B 91 (2008) 71–74.
21. P. Loiko, J. M. Serres, X. Mateos, S. Tacchini, M. Tonelli, S. Veronesi, D. Parisi, A. Di Lieto, K. Yumashev, U. Griebner, V. Petrov, Comparative spectroscopic and thermo-optic study of Tm:$LiLnF_4$ (Ln = Y, Gd, and Lu) crystals for highly-efficient microchip lasers at ~2 μm, Opt. Mater. Express 7 (2017) 844–854.
22. B. M. Walsh, N. P. Barnes, and B. Di Bartolo, Branching ratios, cross sections, and radiative lifetimes of rare earth ions in solids: Application to Tm^{3+} and Ho^{3+} ions in $LiYF_4$, J. Appl. Phys. 3 (1998) 2772–2787.
23. R. Faoro, M. Kadankov, D. Parisi, S. Veronesi, M. Tonelli, V. Petrov, U. Griebner, M. Segura, X. Mateos, Passively Q-switched Tm:YLF laser,"Opt. Lett. 37 (2012) 1517-1519.
24. J. A. Caird, S. A. Payne, P. R. Staber, A. J. Ramponi, L. L. Chase, W. F. Krupke, Quantum electronic properties of the $Na_3Ga_2Li_3F_{12}$:Cr^{3+} laser, IEEE J. Quantum Electron. 24 (1988) 1077–1099.
25. J. Liu, V. Petrov, H. Zhang, J. Wang, Power scaling of a continuous-wave and passively Q-switched Yb:$KLu(WO_4)_2$ laser end-pumped by a high-power diode, Appl. Phys. B 88 (2007) 527-530.

26. J. M. Serres, P. Loiko, X. Mateos, K. Yumashev, U. Griebner, V. Petrov, M. Aguiló, and F. Díaz, "Tm:KLu(WO_4)$_2$ microchip laser Q-switched by a graphene-based saturable absorber," Opt. Express 23(11), 14108–14113 (2015).
27. A. E. Siegman, Lasers. Univ. Sci. Books, Mill Valley, CA, 1986, pp. 1024–1028.
28. S. Chénais, F. Balembois, F. Druon, G. Lucas-Leclin, P. Georges, Thermal lensing in diode-pumped ytterbium lasers-part II: evaluation of quantum efficiencies and thermo-optic coefficients, IEEE J. Quantum Electron. 40 (2004) 1235-1243.
29. J. M. Serres, P. A. Loiko, X. Mateos, V. Jambunathan, A. S. Yasukevich, K. V. Yumashev, V. Petrov, U. Griebner, M. Aguiló, F. Díaz, Passive Q-switching of Tm,Ho:KLu(WO_4)$_2$ microchip laser by a Cr:ZnS saturable absorber, Appl. Opt. 55 (2016) 3757-3763.
30. R. Lan, P. Loiko, X. Mateos, Y. Wang, J. Li, Y. Pan, S. Y. Choi, M. H. Kim, F. Rotermund, A. Yasukevich, K. Yumashev, U. Griebner, V. Petrov, Passive Q-switching of microchip lasers based on Ho:YAG ceramic, Appl. Opt. 55 (2016) 4877–4887.
31. J. H. Lee, S. Gross, B. V. Cunning, C. L. Brown, D. Kielpinski, T. M. Monro, D. G. Lancaster, Graphene-based passive Q-switching of a Tm^{3+}:ZBLAN short-infrared waveguide laser, in Conference on Lasers and Electro-Optics (CLEO) (IEEE, 2014), p. P. JTu4A.128.
32. Y. Ren, G. Brown, R. Mary, G. Demetriou, D. Popa, F. Torrisi, A. C. Ferrari, F. Chen, A. K. Kar, 7.8-GHz graphene-based 2-μm monolithic waveguide laser, IEEE J. Sel. Top. Quantum Electron. 21 (2015) 395– 400.
33. E. Kifle, P. Loiko, J. R. V. de Aldana, C. Romero, A. Ródenas, V. Zakharov, A. Veniaminov, H.i Yu, H. Zhang, Y. Chen, M. Aguiló, F. Díaz, U. Griebner, V. Petrov, X. Mateos, Fs-laser-written thulium waveguide lasers Q-switched by graphene and MoS_2, Opt. Express 27 (2019) 8745-8755.
34. E. Kifle, P. Loiko, J. R. V. de Aldana, A. Ródenas, S. Y. Choi, F. Rotermund, V. Zakharov, A. Veniaminov, M. Aguiló, F. Díaz, U. Griebner, V. Petrov, X. Mateos, Passively Q-switched fs-laser-written thulium waveguide laser based on evanescent field interaction with carbon nanotubes, Phot. Res. 6 (2018) 971-980.
35. X. Jiang, S. Gross, H. Zhang, Z. Guo, M. J. Withford, A. Fuerbach, Bismuth telluride topological insulator nanosheet saturable absorbers for q-switched mode-locked Tm:ZBLAN waveguide lasers, Ann. Phys. 528 (2016) 543–550.
36. J.M. Serres, X. Mateos, P. Loiko, K. Yumashev, N. Kuleshov, V. Petrov, U. Griebner, M. Aguiló, F. Díaz, "Diode-pumped microchip Tm:KLu(WO_4)$_2$ laser with more than 3 W of output power, Opt. Lett. 39 (2014) 4247-4250.
37. J. Song, C. Li, K.I. Ueda, Thermal influence of saturable absorber in passively Q-switched diode-pumped cw Nd:YAG/Cr^{4+}:YAG laser, Opt. Commun. 177 (2000) 307-316.
38. A. Sennaroglu, Continuous-wave power transmission and thermal lensing of a saturable absorber subject to excited-state absorption, Appl. Opt. 38 (1999) 3334-3337.
39. P.A. Loiko, K.V. Yumashev, N.V. Kuleshov, G.E. Rachkovskaya, and A.A. Pavlyuk, Thermo-optic dispersion formulas for monoclinic double tungstates KRe(WO_4)$_2$ where Re = Gd, Y, Lu, Yb, Opt. Mater. 33 (2011) 1688-1694.
40. R.J. Harris, G.T. Johnston, G.A. Kepple, P.C. Krok, H. Mukai, Infrared thermooptic coefficient measurement of polycrystalline ZnSe, ZnS, CdTe, CaF_2, and BaF_2, single crystal KCl, and TI-20 glass, Appl. Opt. 16 (1977) 436-438.

41. J.S. Browder, S.S. Ballard, Thermal expansion data for eight optical materials from 60 K to 300 K, Appl. Opt. 16 (1977) 3214-3217.
42. S.B. Mirov, V.V. Fedorov, K. Graham, I.S. Moskalev, V.V. Badikov, V. Panyutin, Erbium fiber laser–pumped continuous-wave microchip Cr^{2+}:ZnS and Cr^{2+}:ZnSe lasers, Opt. Lett. 27 (2002) 909-911.

List of figure captions

Figure 1. Confocal microscope image of Tm^{3+}:$LiYF_4$ waveguides produced by diamond-saw dicing of LPE-grown thin films (top view).

Figure 2. Scheme of the PQS Tm^{3+}:$LiYF_4$ waveguide laser: λ/2 – rotatory half-wave plate, P – Glan-Taylor polarizer, L – lens, PM – pump mirror, SA – saturable absorber, OC – output coupler, F – cut-off filter.

Figure 3. Ground-state absorption cross-sections, σ_{GSA}, for Cr^{2+} and Co^{2+} ions in the ZnSe crystal. The *vertical line* indicates the laser wavelength (1.88 μm).

Figure 4. PQS Tm^{3+}:$LiYF_4$ waveguide laser: (a) input-output dependences, η – slope efficiency; (b) typical laser emission spectra measured at P_{abs} = 1.5 W. T_{OC} = 50%, the laser polarization is π.

Figure 5. Pulse characteristics of the PQS Tm^{3+}:$LiYF_4$ waveguide laser: (a) pulse duration (FWHM) and pulse repetition frequency (PRF) and (b) pulse energy. T_{OC} = 50%.

Figure 6. Oscilloscope traces of (a) the shortest switched pulses and (b) the corresponding pulse trains for the Tm^{3+}:$LiYF_4$ waveguide laser PQS by Cr^{2+}:ZnSe and Co^{2+}:ZnSe SAs. P_{abs} = 1.67 W.

Figure 7. Calculated (a) pulse duration and (b) energy for the Tm^{3+}:$LiYF_4$ WG laser PQS by a Cr^{2+}:ZnSe SA: T_{OC} – output coupling, T_{SA} – small-signal transmission of the SA. *Circles* – experimental data.

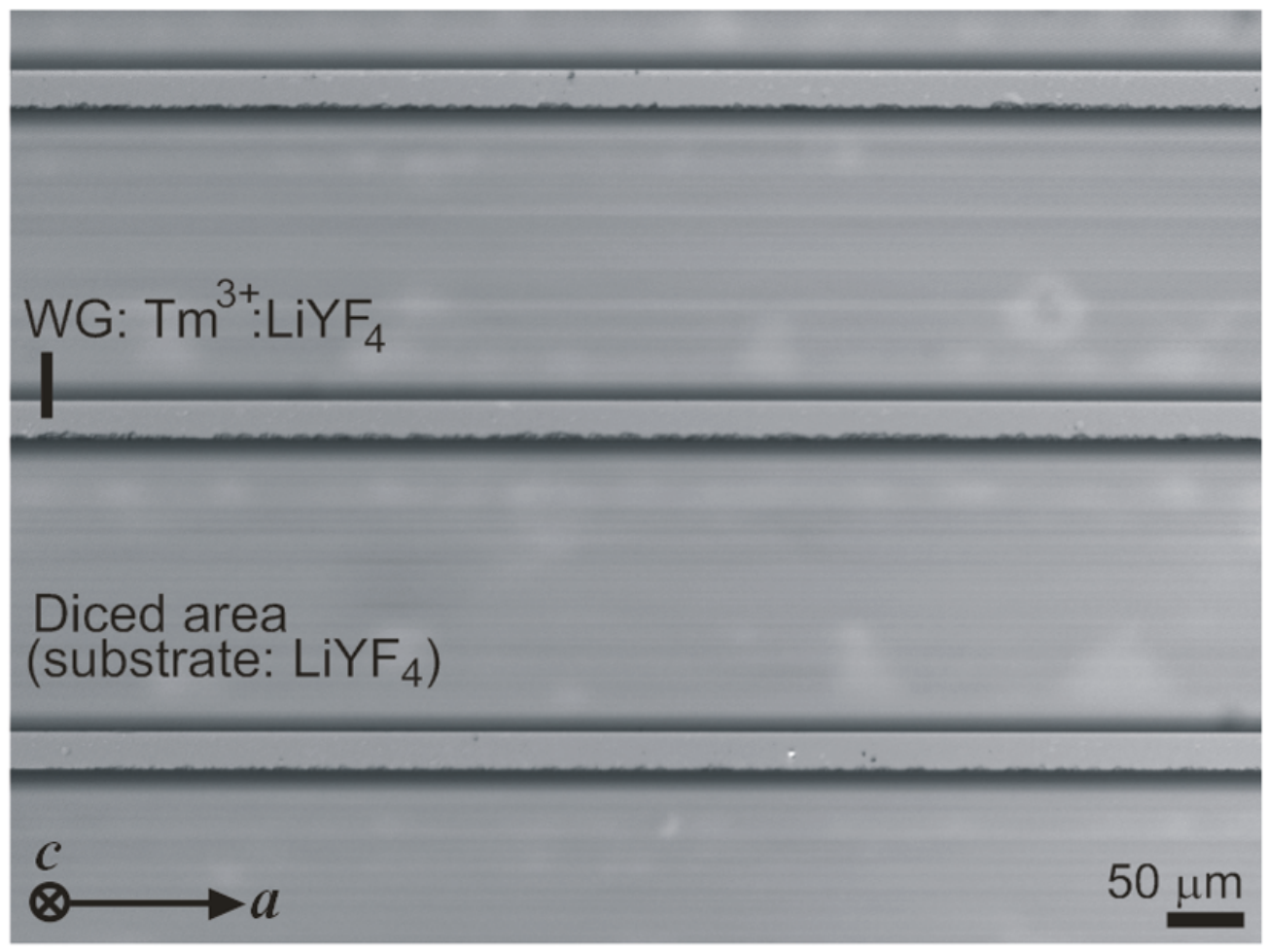
WG: Tm^{3+}:$LiYF_4$
Diced area
(substrate: $LiYF_4$)
c
a
50 μm

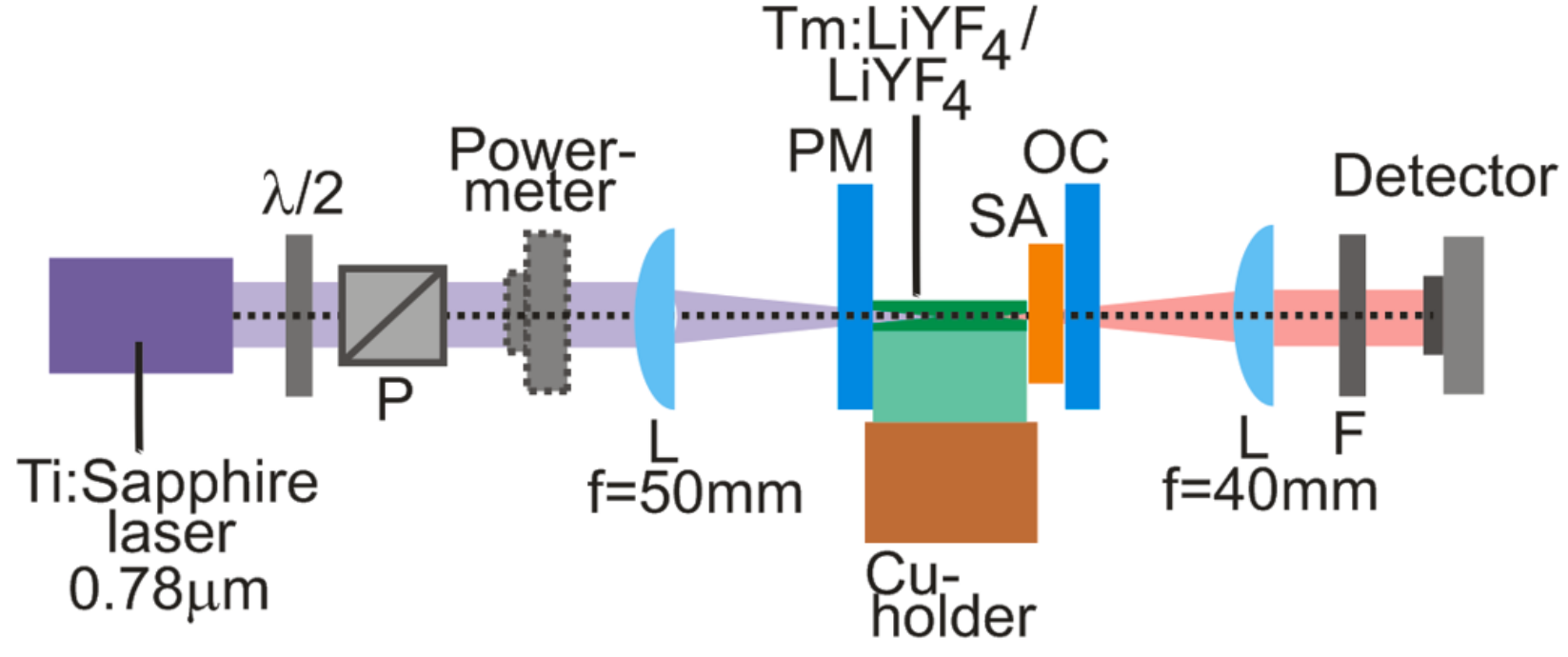
Tm:LiYF4 /
LiYF4
PM
OC
SA
Power-
meter
λ/2
Detector
P
L
f=50mm
L
f=40mm
F
Ti:Sapphire
laser
0.78μm
Cu-
holder

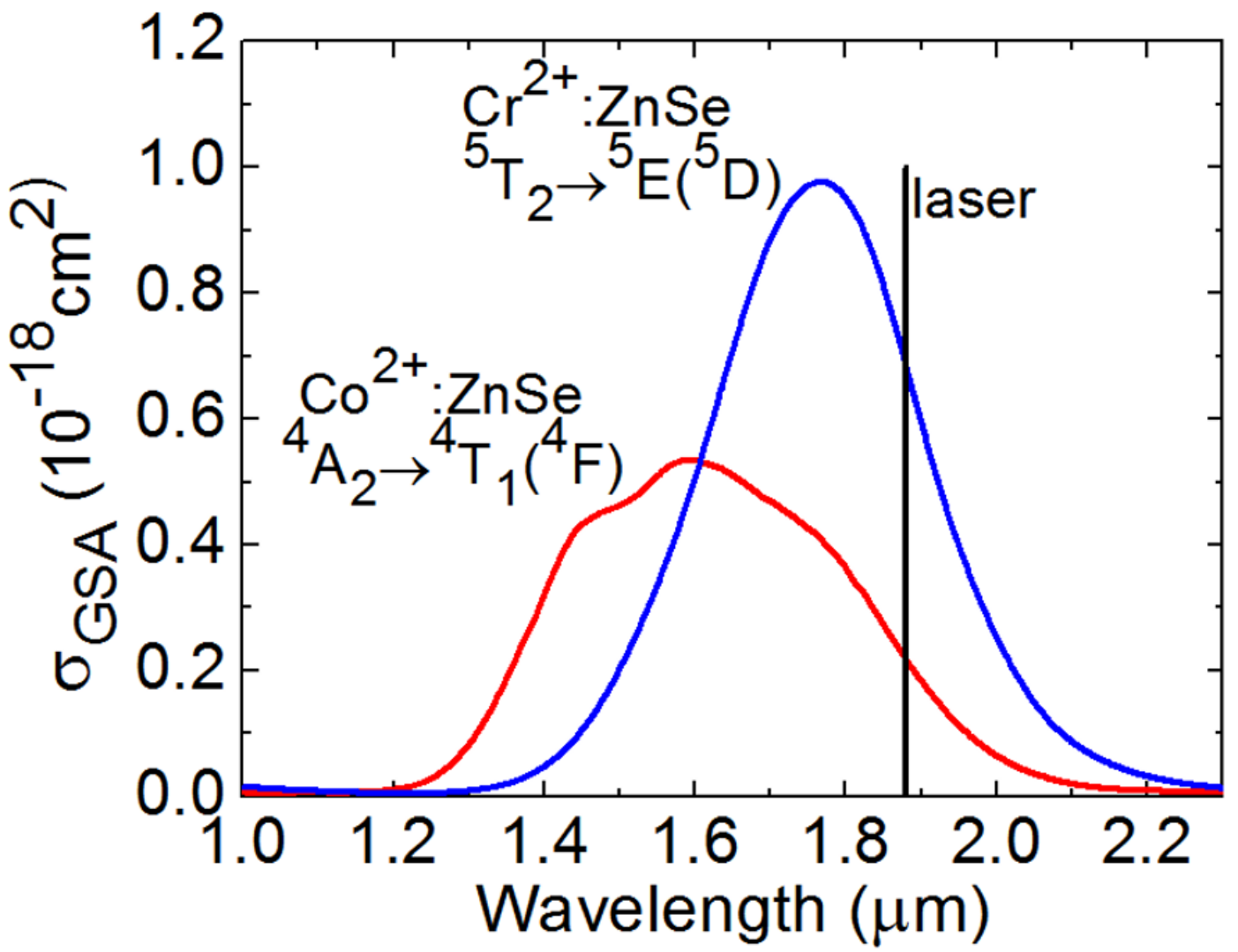
Cr^{2+}:ZnSe
$^5T_2 \rightarrow {}^5E(^5D)$
laser
Co^{2+}:ZnSe
$^4A_2 \rightarrow {}^4T_1(^4F)$
σ_{GSA} (10^{-18}cm^2)
Wavelength (μm)
0.0
0.2
0.4
0.6
0.8
1.0
1.2
1.0
1.2
1.4
1.6
1.8
2.0
2.2

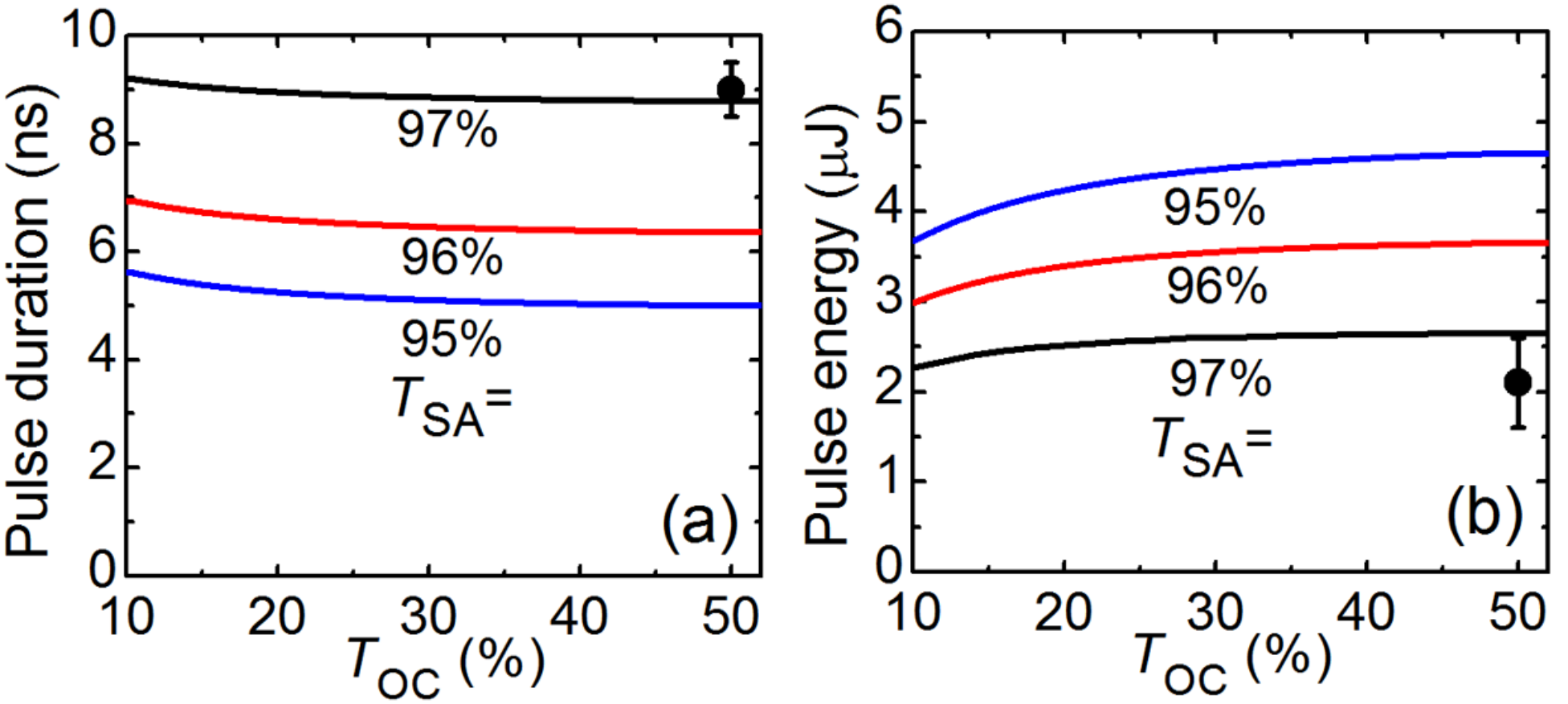
Pulse duration (ns)
10
8
6
4
2
0
97%
96%
95%
T_{SA}=
(a)
10
20
30
40
50
T_{OC} (%)
Pulse energy (μJ)
6
5
4
3
2
1
0
95%
96%
97%
T_{SA}=
(b)
10
20
30
40
50
T_{OC} (%)

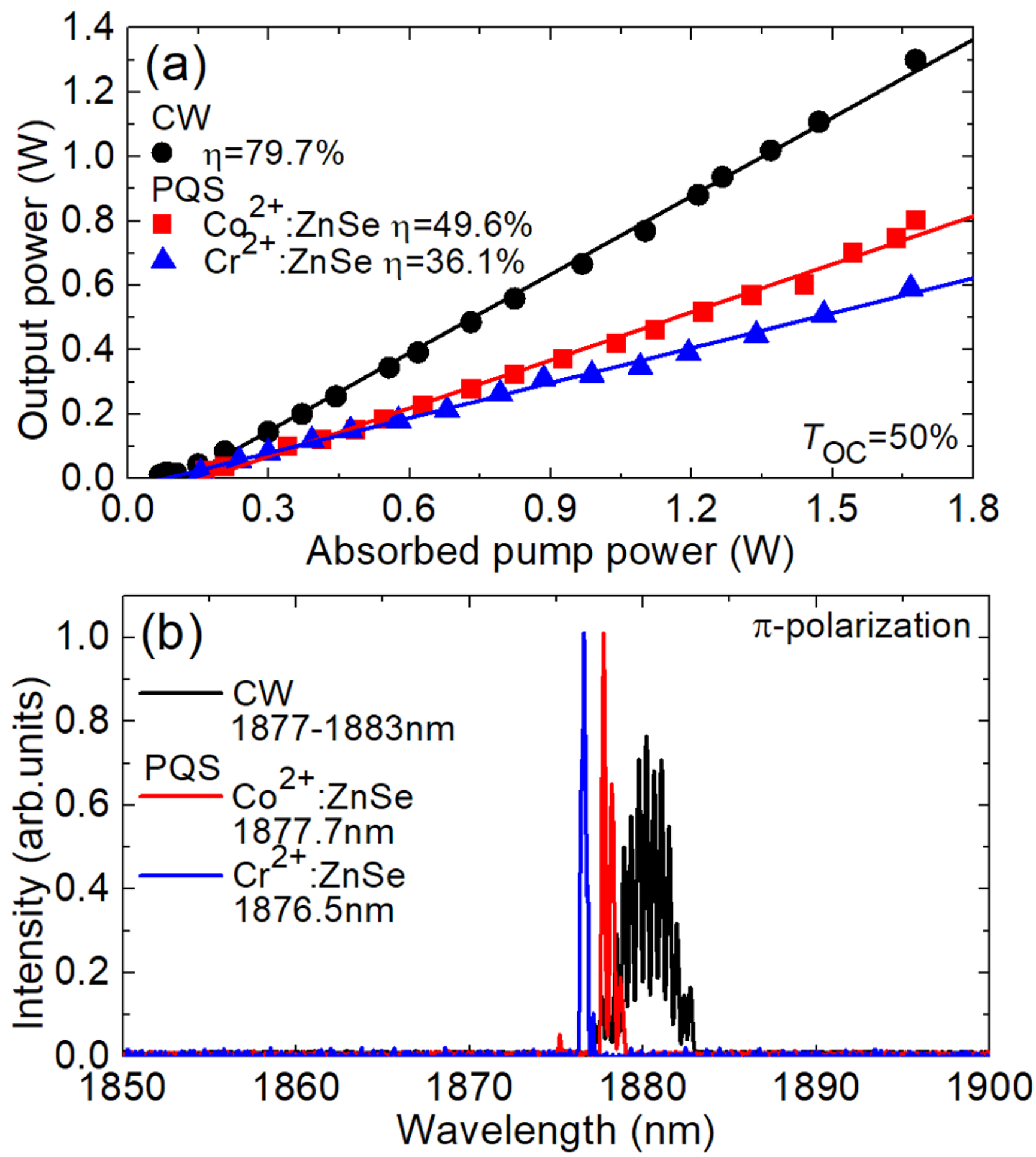
(a)
CW
η=79.7%
PQS
Co2+:ZnSe η=49.6%
Cr2+:ZnSe η=36.1%
TOC=50%
Output power (W)
Absorbed pump power (W)
0.0
0.2
0.4
0.6
0.8
1.0
1.2
1.4
0.0
0.3
0.6
0.9
1.2
1.5
1.8
(b)
π-polarization
CW
1877-1883nm
PQS
Co2+:ZnSe
1877.7nm
Cr2+:ZnSe
1876.5nm
Intensity (arb.units)
Wavelength (nm)
0.0
0.2
0.4
0.6
0.8
1.0
1850
1860
1870
1880
1890
1900

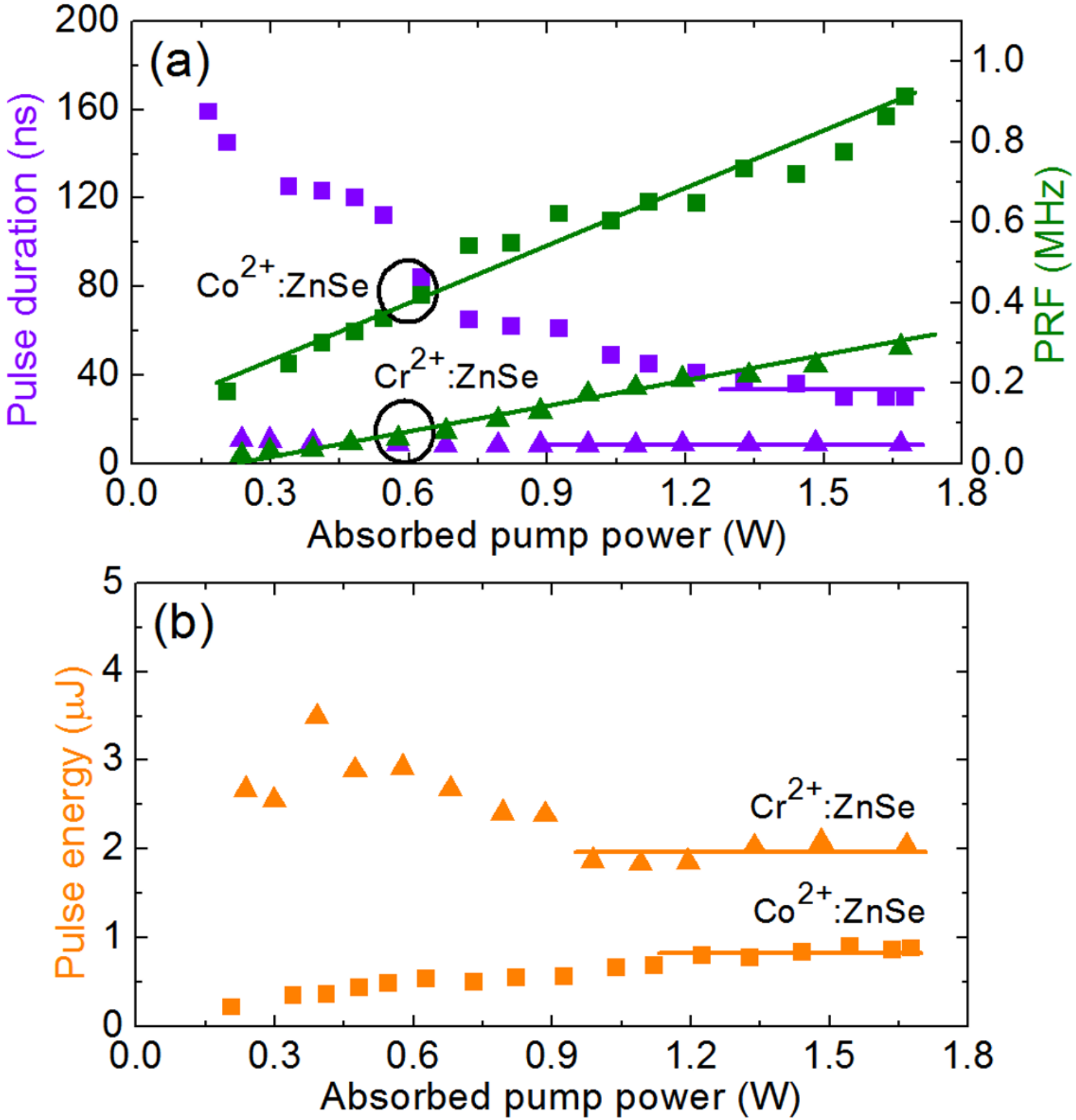
(a)
Pulse duration (ns)
PRF (MHz)
Absorbed pump power (W)
Co2+:ZnSe
Cr2+:ZnSe
(b)
Pulse energy (μJ)
Absorbed pump power (W)
Cr2+:ZnSe
Co2+:ZnSe

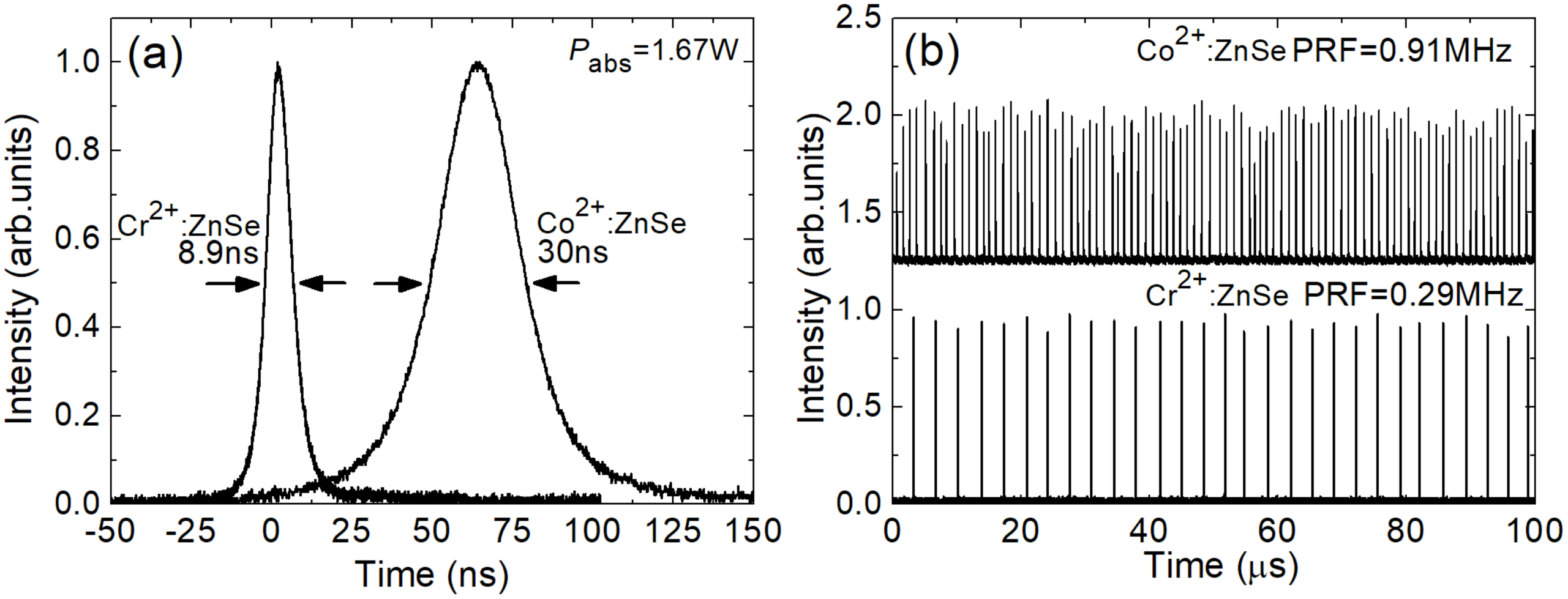
(a)
P_{abs}=1.67W
Cr^{2+}:ZnSe
8.9ns
Co^{2+}:ZnSe
30ns
Intensity (arb.units)
Time (ns)
(b)
Co^{2+}:ZnSe PRF=0.91MHz
Cr^{2+}:ZnSe PRF=0.29MHz
Intensity (arb.units)
Time (μs)

Table 1. Characteristics of Cr^{2+}:ZnSe and Co^{2+}:ZnSe saturable absorbers*.

SA	t, mm	σ_{GSA}, 10^{-18} cm^2	F_S**, J/cm^2	$\sigma_{ESA}/\sigma_{GSA}$	τ_{rec}, μs	T_{SA}, %	Ref.
Cr^{2+}:ZnSe	1.01	0.69	0.15	~0.05	5.4	97.0	[16]
Co^{2+}:ZnSe	1.91	0.22	0.48	<0.05	~100	99.2	[18,19]

*At the laser wavelength of ~1.88 μm.

**Saturation fluence: $F_S = h\nu_L/\sigma_{GSA}$, h –Planck constant, ν_L – laser frequency.

Table 2. Output characteristics* of passively Q-switched Thulium channel waveguide lasers reported so far.

Material	Method **	SA	P_{out}, mW	λ_L, μm	η, %	$\Delta\tau_p$, ns	E_{out}, nJ	PRF, MHz	Ref.
Tm^{3+}:ZBLAN	DLW	graphene	6	~1.9	~5	2760	240	0.025	[31]
		Bi_2Te_3	16.3	1.88	1.3	1400	370	0.044	[35]
Tm^{3+}:$Y_3Al_5O_{12}$	DLW	graphene	6.5	1.94	~2	<500	9.5	0.68	[32]
Tm^{3+}:$KLu(WO_4)_2$	DLW	SWCNT***	150	1.85	34.6	98	106	1.42	[34]
		graphene	24.9	1.84	9.3	88	18	1.39	[33]
		MoS_2	22.1	1.84	8.5	73	14	**1.58**	[33]
Tm^{3+}:$LiYF_4$	LPE	Cr^{2+}:ZnSe	590	1.88	36.1	**9**	**2100**	0.29	****
		Co^{2+}:ZnSe	**810**	1.88	**49.6**	30	900	0.91	****

*P_{out} – average output power, λ_L – laser wavelength, η – slope efficiency, $\Delta\tau_p$ – pulse duration, E_{out} – pulse energy, PRF – pulse repetition frequency.

**Fabrication method: DLW – femtosecond Direct Laser Writing, LPE – Liquid Phase Epitaxy and diamond-saw dicing.

***SWCNT – single-walled carbon nanotubes.

****This work.